

CHALLENGES IN THE THERMAL MODELING OF HIGHLY POROUS CARBON FOAMS

A. FEHÉR¹, R. KOVÁCS^{1,2,3}, Á. SUDÁR², G. G. BARNAFÖLDI²

ABSTRACT. The heat pulse experiment is a well-known, widely used method to determine the thermal diffusivity. However, for heterogeneous, highly porous materials neither the measurement nor the evaluation methodologies are straightforward. In the present paper we focus on two open-cell carbon foam types, differing in their porosity but having the same size. Recent experiments showed that a non-Fourier behaviour, called 'over-diffusive' propagation is probably present for such a complex structure. The (continuum) Guyer–Krumhansl equation stands as a promising candidate to model such transient thermal behaviour. In order to obtain a reliable evaluation and thus reliable thermal parameters, we utilize a novel, state-of-the-art evaluation procedure, developed recently using an analytical solution of the Guyer–Krumhansl equation. Based on our observations, it turned out that the presence of high porosity alone is a necessary but not satisfactory for non-Fourier behaviour. Additionally, the mentioned non-Fourier effects are porosity-dependent, however porous samples can also follow the Fourier law. These data serve as a basis to properly identify the characteristic heat transfer mechanisms and their corresponding time scales, which altogether result in the present non-Fourier behaviour.

Keywords: flash experiments, non-Fourier heat conduction, highly porous carbon foams.

1. INTRODUCTION

Together with the development of advanced manufacturing technologies, materials with complex inner structure appeared in the engineering practice. The one we place the focus on is an open-cell, highly porous carbon foam material, which has particular mechanical and thermal properties. Its lightweight, highly porous structure promotes that material to be exceptional in applications requiring large surface / volume (or mass) ratio such as supercapacitors [1] and chemical synthesis [2]. Besides, that material type is also outstandingly advantageous for particle detectors, especially in large-scale detectors, where the low material budget is a key factor. In that case, less mass density means much less probability for unwanted particle scattering and that greatly increases the reliability and accuracy for sensors being attached onto that structure. As these semiconductors also dissipate power, they need cooling, which can be more efficient thanks to the open-cell design of the foam, while having acceptable mechanical stability. In the following, we provide a brief introduction about the specific aspects we focus on in the present study.

1.1. Low material budget detectors. One of the novelty of recent detector developments in High Energy Physics (HEP) is to build detectors with as low material budget as possible. A lightweight detector setup absorbs less particle, therefore it can measure more details of the elementary processes. This novel R&D direction is presented by the application of the thin silicon pixel detectors, where the thickness of a sensor layer is getting close to the $\mathcal{O}(50 \mu\text{m})$ size [3]. Building such a detector required large and solid support frames, with minimal material budget as well. For this aim, application of light material foams can be excellent option, especially the since porosity offers good options for air cooling as well.

As an example, one can see the ALICE detector upgrade plans at the CERN's Large Hadron Collider [4]. The upgrade of the Inner Tracking System (ITS3) is planned for the Long Shutdown 3 (LS3) during the period 2025–2027 [5, 6]. This development will include a new vertex tracker based on truly cylindrical wafer-scale semiconductor sensors with material budget, $< 0.05\% X/X_0$ per layer, and located as close as 18 mm to the interaction point [7, 8]. The performance studies indicate, that the additional 3-layer provide an improvement by a factor 2 of the pointing resolution and of the standalone tracking efficiency down to the lowest momentum regime ($< 100 \text{ MeV}/c$). This opens new window to explore the stages of the high-energy hadron collisions at the early stage [5, 9].

In recent R&D activities, carbon foam samples has been tested in the laboratory beside carbon fibre structures. ALICE has found, that carbon foams are the most promising candidates to satisfy both the low material budget and the cooling requirements, however modelling such structure using finite-element simulations is not suitable as the entire design procedure would be highly resource intensive. Moreover, as such structures can show non-Fourier behaviour, it is worth investigating the effects of porosity. In order to obtain reliable, more precise and resource friendly solutions, we analyse the two, highly porous carbon foam samples to better understand their thermal behaviour and whether the high porosity indeed results non-Fourier effects.

1.2. Heat conduction in foams. A recent study of Lunev et al. [10] presented the complexity of such material from both experimental and thermodynamic modeling point of view. First, they realized that the Fourier heat equation alone is not enough to properly characterize the overall transient behaviour of an aluminium foam material. In order to exclude the possibilities of any experimental artefact, they performed numerous detailed, highly resource intensive simulations. It turned out that the measurements are acceptable and the deviation from Fourier's law is valid. It is worth to emphasize that the separate components obey Fourier's law, however, their interaction during the heat conduction process results in a non-Fourier behaviour.

It is clear that such simulations have enormous computational and memory requirement, needing high-end performance workstations or even clusters to run the simulation. While it can be accurate, the outcomes are valid only for a particular sample, cannot be generalized, and additionally, its energy demand is high and that could be a problem nowadays, being not necessarily feasible.

Regarding the deviation from Fourier's law, we emphasize that this is characteristic on room temperature, macro scale samples with inclusions in the order of millimeters. Such heterogeneous sample can provide a non-Fourier thermal response in the standard heat pulse (flash) measurement technique (see Fig. 1). Additionally, Fourier's law can lead to errors up to 30% for thermal diffusivity, and thus predicts a significantly different temperature profile. Figure 1 presents a typical outcome in that regard, showing that Fourier's law fails to properly model the transient behaviour; first the predicted temperature is slower, then it becomes faster, indicating the presence of two characteristic time scales in heat transfer in natural dimensionless units [13].

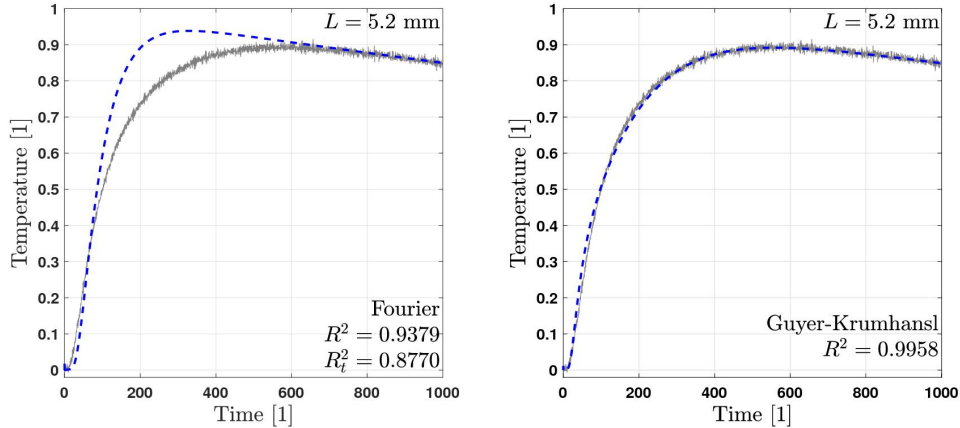


FIGURE 1. Typical experimental temperature history [13]. Left side: Fourier's prediction. Right side: evaluation using the Guyer - Krumhansl equation.

The observations of Lunev et al. are in agreement with previous experiments, which shows the same deviation [11–13], additionally, it is found that Guyer – Krumhansl (GK) equation is a promising candidate to model and explain the observed phenomenon, obtaining a notably better thermal description for that problem. This is a 'double-diffusive' model, consisting two characteristic time scales, therefore it can model the interaction of different heat transfer channels (mechanisms) of foam materials by introducing two new parameters. These can be determined from a single flash experiment together with the thermal diffusivity [13]. The GK equation also provides effective parameters, similarly to Fourier's law, hence no detailed, highly resource intensive simulations are needed as the effective parameters substitute the complex inner structure.

The main difficulty comes with characteristic lengths. All standard measurement equipment are limited for a thickness of three to five millimeters, therefore the sample is not necessarily representative in regard to the heterogeneity it consists, resulting in a probable size dependence [14]. This is still an open question, and with exploring these difficulties, we have a step closer in the development of novel measurement techniques. However, at this moment, we can only apply the standard technique to measure the thermal diffusivity with keeping in mind the possible shortcomings.

In the following, we provide a short overview for the experimental and modeling background we use, then we present and discuss our findings about the thermal behaviour of carbon foam samples.

2. MODELS AND EVALUATION FOR HEAT PULSE EXPERIMENTS

2.1. Experimental arrangement. The experiments are carried out using a well-known and used flash heat pulse method, which allows the determination of the thermal diffusivity, for our purpose, room temperature measurements

are satisfactory. The arrangement of the experiment is shown in Fig. 2. The excitation is provided by a flash lamp on the front face of the heterogeneous sample, while the temperature history is measured on the rear face using a K-type thermocouple. The thermocouple outputs are isolated during the measurement in order to minimize the various electrical noises and to prevent the heat pulse source from introducing any disturbance into the thermocouple circuit and thus into the measurement itself. An important part of the measurement is the trigger signal, the signal that shows exactly when the heat pulse occurred. This is detected and recorded by a photovoltaic sensor that induces a voltage in response to light. The measured signals are recorded with a PC oscilloscope. The advantage of the oscilloscope is that peaks due to interference can be reduced using gain settings.

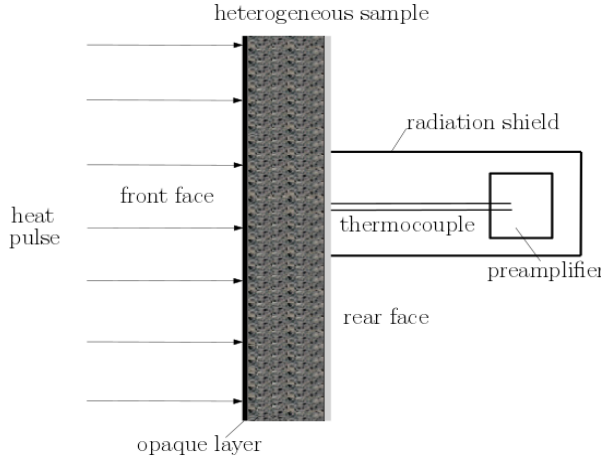


FIGURE 2. Arrangement of the experimental setup for the heat-pulse measurement of carbon foam samples.

The samples used in the experiments are $10 \times 10 \times 5$ mm³ brick blocks with a random internal structure, and produced by the ERG Aerospace Corporation and Allcomp Inc. Two types of samples were measured, which are geometrically identical but differ in their internal structure. The higher porosity sample is called ERG, while the denser one is called AllCompLD Standard. The difference between the two samples is shown in Figure 3. The porosity of the ERG sample is 0.97, while the porosity of the AllCompLD Standard samples varies between 0.85 and 0.9, depending on the samples.

It can be seen that both types are transparent, so measuring them without any preparation can give false results. For this reason, a sheet of graphite-coated paper is attached on the front side before the experiments begin. Hence the heat pulse can be absorbed on the front face while the thermal resistance of the impregnated paper has negligible impact on the overall behaviour since it has practically the same thermal conductivity as the foam matrix but with a thickness being one magnitude smaller than the sample. Otherwise, the sample would be too transparent for the thermal radiation and the absorption would not be homogeneous on the front surface, thus such measured data cannot be interpreted.

2.2. Guyer – Krumhansl constitutive equation. The main building blocks of thermodynamics are the balance equations represented by the balance of initial energy $e = cT$ with c being the specific heat and ρ is the mass density, and reads as

$$\rho c \partial_t T + \partial_x q = 0, \quad (1)$$

for heat conduction in solid bodies without heat sources and mechanical coupling. All these coefficients are constant, assumed to be independent of temperature, only rigid bodies are assumed. To close the balance equation of energy (1) one needs to define a so-called constitutive equation in accordance with second law of thermodynamics. The usual candidate is the Fourier's equation, which describes well most of the room temperature measurements, except some of the recent observations in heterogeneous samples. In these cases the Guyer – Krumhansl equation was found to be the least necessary extension of Fourier's law, which reads in one spatial dimension

$$\tau_q \partial_t q + q + \lambda \partial_x T - \kappa^2 \partial_{xx} q = 0. \quad (2)$$

Here, τ_q is the relaxation time for the heat flux q and κ^2 is a kind of 'dissipation parameter'. Whereas it was first derived on the basis of kinetic theory [15], this model also has a strong background in non-equilibrium thermodynamics with internal variables (NET-IV), in which the new coefficients originate from the Onsagerian relations, and are restricted by the second law [16,17]. Moreover, since the derivation of the GK equation exploits the energy

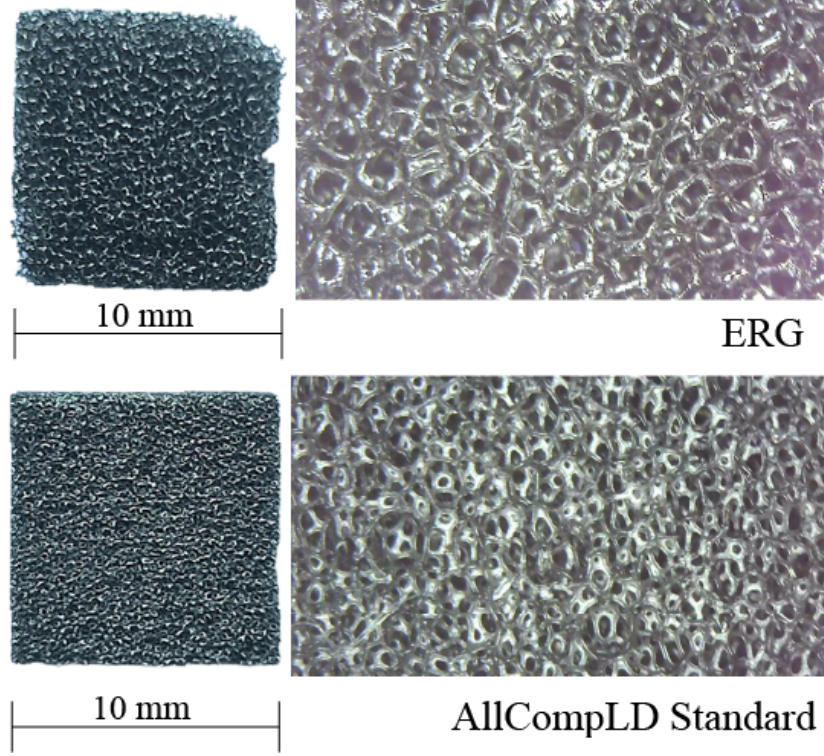


FIGURE 3. Carbon foam samples: ERG (upper) and AllCompLD (lower) samples with $500\times$ magnification by optical microscope.

balance (1) as a constraint, (1) is naturally satisfied. It is crucial to emphasize that continuum GK equation (2) is free from any assumption on the microscopic mechanisms, therefore this model is free from the usual limitations and it is applicable for room temperature problems with very low Knudsen number, too.

The advanced evaluation procedure we are using is built on the dimensionless form of the governing equations,

$$\partial_t T + \partial_x q = 0, \quad (3a)$$

$$q + \alpha \partial_x T = 0, \quad (3b)$$

$$\tau_q \partial_t q + q + \alpha \partial_x T - \kappa^2 \partial_{xx} q = 0. \quad (3c)$$

together with the parameters defined in Table 1, following [11,13]. In what follows, we neglect the hat notation and we use dimensionless parameters by default. We explicitly denote the units if necessary.

$$\begin{aligned}
 \text{Time and spatial coordinates:} \quad & \hat{t} = \frac{t}{t_p} & \text{and} & \hat{x} = \frac{x}{L} \\
 \text{Thermal diffusivity:} \quad & \hat{\alpha} = \frac{\alpha t_p}{L^2} & \text{with} & \alpha = \frac{\lambda}{\rho c} \\
 \text{GK parameters:} \quad & \hat{\tau}_q = \frac{\tau_q}{t_p} & \text{and} & \hat{\kappa}^2 = \frac{\kappa^2}{L^2} \\
 \text{Temperature:} \quad & \hat{T} = \frac{T - T_0}{T_{\text{end}} - T_0} & \text{with} & T_{\text{end}} = T_0 + \frac{\bar{q}_0 t_p}{\rho c L} \\
 \text{Heat flux:} \quad & \hat{q} = \frac{q}{\bar{q}_0} & \text{with} & \bar{q}_0 = \frac{1}{t_p} \int_0^{t_p} q_0(t) dt \\
 \text{Heat transfer coefficient:} \quad & \hat{h} = h \frac{t_p}{\rho c} \\
 \text{Fourier resonance condition:} \quad & \hat{\kappa}^2 / \hat{\tau}_q = \hat{\alpha}
 \end{aligned}$$

TABLE 1. Dimensionless quantities following [11,13], where t_p denotes the heat pulse duration for which interval \bar{q}_0 averages the heat transferred by the heat pulse. Here, L is the sample thickness. T_{end} represents the adiabatic steady-state, and T_0 is the uniform initial temperature.

2.3. Evaluation of heat pulse measurements. At this point the authors followed the method published and described in detail in [13], which is shortly summarized here for completeness. This technique uses the Galerkin method to provide an analytical solution for the system of balance (3a) and the Fourier (3b) / GK (3c) equations, resulting in such analytical formulas that can be simplified enough to immediately determine the necessary parameters. Moreover, that approach accounts the finite length and shape of the pulse as well, including heat transfer with the environment.

The heat transfer coefficient h is determined by reading dimensionless temperature-time instant pairs as

$$h = -\frac{\ln(T_2/T_1)}{t_2 - t_1}. \quad (4)$$

The corresponding pairs are picked from the rear side of the curve as heat conduction is no more dominating the behaviour, only heat transfer to the environment is present.

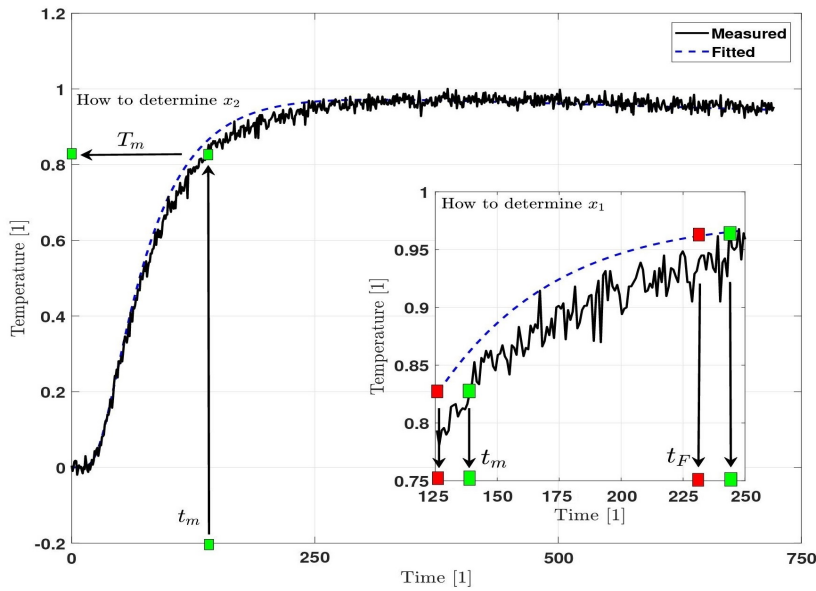


FIGURE 4. The schematic representation of the evaluation method using the Guyer–Krumhansl theory. Here, the 'fitted curve' (dashed line) has been given by the Fourier equation and used as a reference to introduce the proper correction factor in Eq. (8) in natural, dimensionless units.

We start the evaluation with Fourier equation as it describes most of the room temperature measurements well, and also provides a reference for the GK equation when needed. The corresponding (dimensionless) approximate Fourier-solution for the rear side temperature history is

$$T(x = 1, t > 40) = Y_0 \exp(-ht) - Y_1 \exp(x_F t), \quad x_F = -2h - \alpha\pi^2, \quad (5)$$

where x_F describes the characteristic time scale based on Fourier's law. Here, the thermal diffusivity α can immediately be estimated in the classical way, i.e.,

$$\alpha_F = 1.38 \frac{L^2}{\pi^2 t_{1/2}}, \quad (6)$$

where $t_{1/2}$ is the time measured in seconds to reach the half T_{end} , the adiabatic steady-state temperature. Then, α_F can be easily changed to its dimensionless form as the pulse length and sample thickness are known parameters. Hence, all the necessary parameters are known and can be fine tuned to achieve the best fit to the given experimental data.

In case when Fourier's law fails to properly model the measured data, we proceed with the GK equation, the corresponding approximate solution reads

$$T(x = 1, t > 40) = Y_0 \exp(-ht) - Z_1 \exp(x_1 t) - Z_2 \exp(x_2 t), \quad x_1, x_2 < 0, \quad (7)$$

where x_1 and x_2 are characterizing the two time scales, thus introducing the necessary corrections to provide a more precise and reliable thermal parameters. First,

$$x_1 \approx x_F \frac{t_{F1} - t_{F2}}{t_{m1} - t_{m2}}, \quad (8)$$

where t_{m1} and t_{m2} are the time instants of the data, and t_{F1} and t_{F2} are the reference time instants corresponding to the same temperature (see Fig. 4). This is the leading order correction, $|x_2| \gg |x_1|$, thus the second exponential term is approximately zero after $t > 200$, and Z_1 is determined on that basis:

$$Z_{1,m} = \frac{\left(T_m - Y_0 \exp(-ht_m) \right)}{-\exp(-x_{1,m} t_m)}. \quad (9)$$

The parameters of $Z_2 \exp(-x_2 t)$ term can be determined using $Z_2 = -Z_0 - Z_1$, i.e., Z_1 Z_2 are not independent, where Z_0 has an a-priori value of -2.015 and later fine-tuned in the interval of $2 < -Z_0 < 2.03$, thus x_2 is calculated with the following expression:

$$x_2 = \frac{1}{t} \log \left(\frac{T - Y_0 \exp(-ht) + Z_1 \exp(x_1 t)}{-Z_2} \right). \quad (10)$$

The GK parameters (α , τ_q and κ^2) are determined from the roots of the quadratic equation $x_j^2 + k_{1j}x + k_{2j} = 0$:

$$x_{1,2} = x_{j1,2} | j = 1, \quad x_{j1,2} = \frac{1}{2} \left(-k_{1j} \pm \sqrt{k_{1j}^2 - 4k_{2j}} \right), \quad k_{1j} = \frac{1 + \kappa^2 j^2 \pi^2}{\tau_q} + 2h, \quad k_{2j} = \frac{\alpha j^2 \pi^2}{\tau_q} + \frac{2h}{\tau_q}. \quad (11)$$

The parameters are determined on a set of measurement points and averaged. As a final step, sweep is required through $2.00 - 2.03$ values with $-Z_0$ to determine the proper values of α , τ_q and κ^2 . For more technical details, we refer again to [13].

3. EXPERIMENTAL FINDINGS

We thoroughly investigated the obtained measurement data on the ERG and AllCompLD samples. Both models, Fourier and GK, have been applied on the measured data. Here we summarize the obtained result by testing the models' performance.

ERG samples. It is found that the ERG sample with looser structure does not show any non-Fourier phenomenon, Fourier equation is proved to be appropriate for all the three samples we received and measured. The corresponding thermal diffusivity values are summarized in Table 2, found as an average of multiple measurements on three different ERG samples. The notable difference between ERG.1 and the others possibly originating from the different structure as the porosity levels cannot be the same. Figure 5 shows a typical outcome for an ERG sample.

Sample ID	α_F $10^{-7} [\text{m}^2/\text{s}]$
ERG.1	6.06 ± 0.12
ERG.2	7.45 ± 0.19
ERG.3	7.37 ± 0.54

TABLE 2. Thermal diffusivity of the ERG samples by the Fourier equation.

Sample ID	α_F 10^{-6} [m ² /s]	α_{GK} 10^{-6} [m ² /s]	τ_q [s]	κ^2 10^{-6} [m ²]
AllComp_1	8.25 ± 0.74	6.9 ± 0.45	0.160 ± 0.005	2.432 ± 0.096
AllComp_2	5.78 ± 0.27	4.55 ± 0.2	0.207 ± 0.032	2.385 ± 0.167

TABLE 3. Thermal diffusivity of the AllCompLD samples.

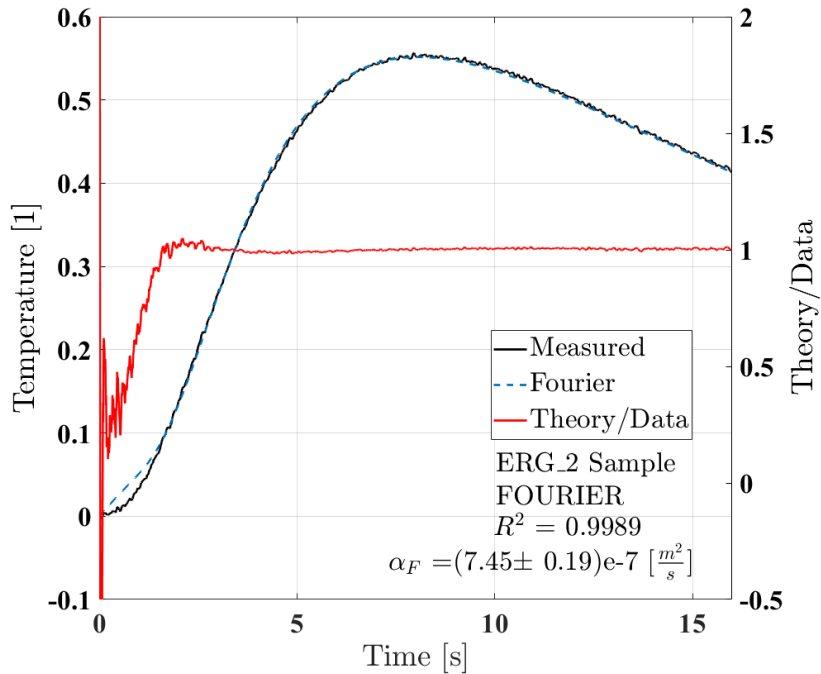


FIGURE 5. ERG_2 sample evaluation with the Fourier theory.

AllCompLD samples. In contrast to the ERG sample, the more dense AllCompLD Standard sample showed non-Fourier behaviour in all cases, the found thermal parameters are summarized in Table 3.

It can be observed that the random internal structure of the samples also strongly influences the thermal diffusivity, so that at such small sizes the samples are not necessarily representative of the material properties. On the other hand, we emphasize again that the capacity of the measuring equipment is limiting the size of the sample, therefore larger number of samples with the same size and porosity would be more conclusive. Furthermore, the Fourier thermal diffusivity is always seem larger than the one found by the GK equation.

The outcome of the AllcompLD_2 sample measurements is shown in Figures 6 and 7. It can be clearly seen that the Fourier fitting was not successful, that model cannot be fitted to the measurement data (Figure 6), producing the same type of deviation that was experiences before in [12]. In such a case, at the beginning of the measurement, Fourier's prediction is slower than the actual temperature measured. Approaching the top, the predicted temperature signal becomes faster than the actual one. After that, typically after 4 s, cooling is dominating the process and therefore both curves run together.

It can be seen that the fit at the beginning of the measurement is also different in the GK case, this may be due to the transparency for thermal radiation, which we could not fully eliminate during the measurements.

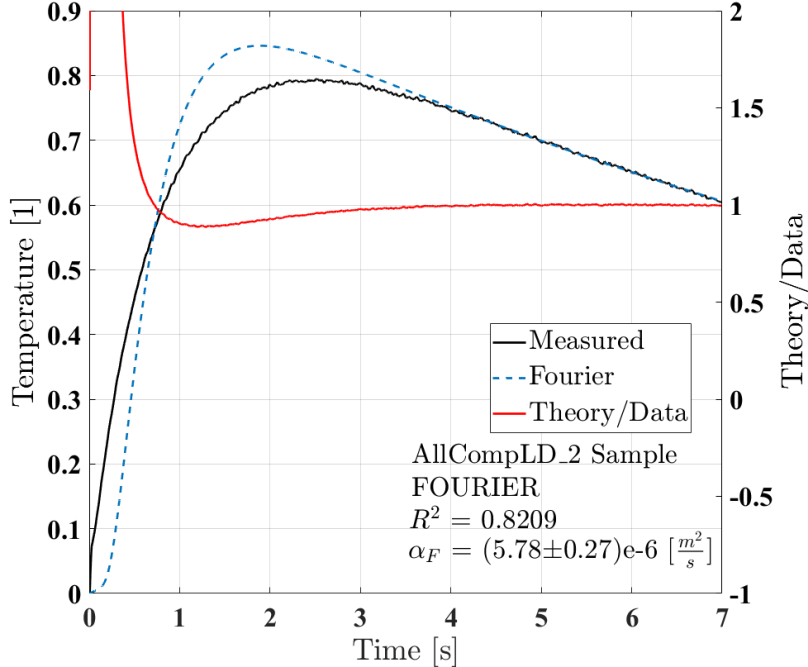


FIGURE 6. AllCompLD_2 sample evaluation with the Fourier theory.

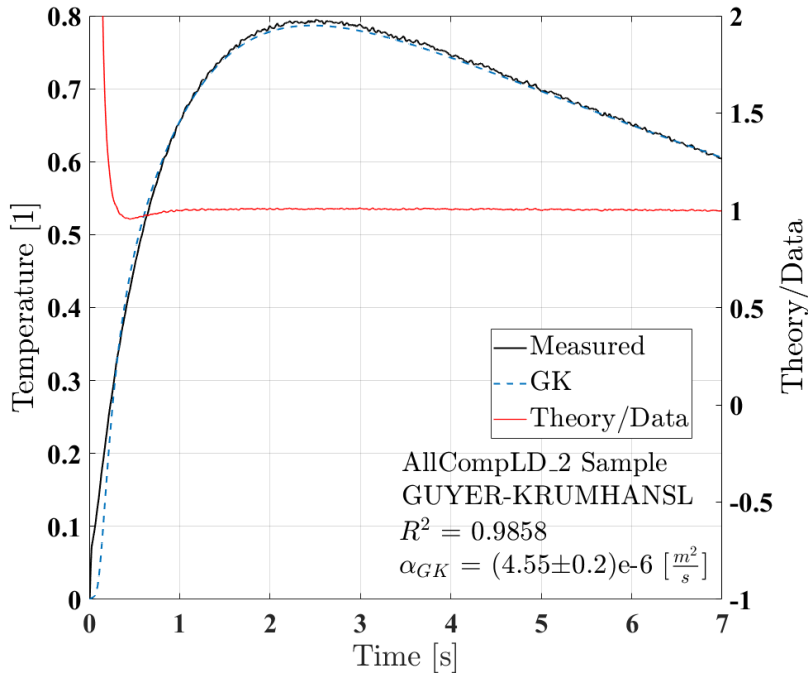


FIGURE 7. AllCompLD_2 sample evaluation with the Guyer-Krumhansl theory.

4. DISCUSSION AND SUMMARY

The heat pulse (flash) experiment has been performed on several, novel carbon foam samples for the first time. Two samples with porosity of 0.97 (ERG) and 0.85-0.90 (AllCompLD) by the ERG Aerospace Corporation and Allcomp Inc. has been measured, respectively. Flash method is a well-known and widely accepted procedure to

measure the thermal diffusivity, however, for foams, the found thermal diffusivity can greatly depend on the structure and on the possible non-Fourier behaviour. We prepared the samples with graphite-coated, impregnated paper to achieve the homogeneous boundary condition for all measurements. The measured data was fitted with the Fourier and the Guyer–Krumhansl heat conduction equations.

First, we obtained that ERG samples follow the Fourier model well, and provide a thermal diffusivity parameter, $\alpha_F = (6.96 \pm 1.02) \times 10^{-7} \text{ m}^2/\text{s}$ ($R^2 = 0.9989$), indeed the Guyer–Krumhansl solution for this sample results in the Fourier limit as well.

In contrary, sample AllCompLD provided non-Fourier behaviour, which significantly detunes the thermal diffusivity. Moreover, it necessitates the use of further parameters, too, which all can be determined using the same temperature history. For Fourier fits, $\alpha_F = (7.02 \pm 1.7) \times 10^{-6} \text{ m}^2/\text{s}$ ($R^2 = 0.8209$). Moreover, the measured data was in good agreement with the Guyer–Krumhansl model with parameters, $\alpha_{GK} = (5.73 \pm 1.5) \times 10^{-6} \text{ m}^2/\text{s}$, $\tau_q = (0.1841 \pm 0.055) \text{ s}$, and $\kappa^2 = (2.41 \pm 0.121) \times 10^{-6} \text{ m}^2$.

Following from these results, we conclude, that finite element calculations can safely be carried out for the ERG sample during the design of the detector. Moreover, it is now possible to perform the necessary simulations effectively, i.e., neglecting the detailed structure and substituting it with a homogeneous one. This saves huge amount of energy and efforts, and greatly decreases the computational costs. Regarding the AllCompLD samples, the situation is more challenging due to the non-Fourier behaviour and the implementation of the Guyer–Krumhansl equation for a finite element environment is still not straightforward. Adding that the parameters show significant porosity dependence, more thorough experimental and theoretical research is needed, e.g., with investigating a wide range of samples with varying porosity levels. Authors are about to continue the measurements with further types and different porosity carbon foam samples.

5. ACKNOWLEDGEMENT

The research reported in this paper and carried out at BME has been supported by the grants National Research, Development and Innovation Office–NKFIH FK 134277, K 135515, 019-2.1.6-NEMZ_KI-2019-00011, and by the NRDI Fund (TKP2020 NC, Grant No. BME-NC) based on the charter of bolster issued by the NRDI Office under the auspices of the Ministry for Innovation and Technology. This paper was supported by the János Bolyai Research Scholarship of the Hungarian Academy of Sciences (KR). Samples were provided by C. Gargiulo and the ALICE Experimental Collaboration (CERN).

REFERENCES

- [1] Lei Zhang and Xaosong Hu and Zhenpo Wang and Fengchun Sun and David G. Dorrell. A review of supercapacitor modeling, estimation, and applications: A control/management perspective. *Renewable and Sustainable Energy Reviews*, 81:1868–1878, 2018.
- [2] Liu, Heguang and Wu, Shaoqing and Tian, Na and Yan, Fuxue and You, Caiyin and Yang, Yang. Carbon foams: 3D porous carbon materials holding immense potential. *J. Mater. Chem. A*, 8(45):23699–23723, 2020.
- [3] M. Mager (On behalf of the ALICE Collaboration), ALPIDE, the Monolithic Active Pixel Sensor for the ALICE ITS upgrade Nuclear Instruments and Methods in Physics Research Section A: Accelerators, Spectrometers, Detectors and Associated Equipment Volume 824, 11 July 2016, Pages 434–438
- [4] <https://alice-collaboration.web.cern.ch/>
- [5] L. Musa, W. Riegler, Letter of Intent for an ALICE ITS Upgrade in LS3, CERN-LHCC-2019-018 ; LHCC-I-034
- [6] M. Šuljić (on behalf of the ALICE Collaboration), The Novel ALICE Inner Tracking System (ITS3) Based on Truly Cylindrical, Wafer-Scale Monolithic Active Pixel Sensors, *JPS Conf. Proc.* 34, 010011 (2021) [8 pages] Proceedings of the 29th International Workshop on Vertex Detectors (VERTEX2020) <https://journals.jps.jp/doi/abs/10.7566/JPSCP.34.010011>
- [7] D. Colella (on behalf of ALICE Collaboration), ALICE ITS 3: the first truly cylindrical inner tracker, proceedings at the 12th International Conference on Position Sensitive Detectors - PSD12 12-17 September, 2021, Birmingham, U.K
- [8] M. Buckland, (on behalf of ALICE collaboration) Development of the ITS3: A bent-silicon vertex detector for ALICE in the LHC Run 4, *Nuclear Inst. and Methods in Physics Research, A* 1039 (2022) 166875
- [9] L. Musa, W. Riegler, Letter of intent for ALICE 3: A next generation heavy-ion experiment at the LHC, CERN-LHCC-2022-009 ; LHCC-I-038
- [10] A. Lunev and A. Lauerer and V. Zborovskii and F. Léonard. Digital twin of a laser flash experiment helps to assess the thermal performance of metal foams. *International Journal of Thermal Sciences*, 181:107743, 2022.
- [11] S. Both, B. Czél, T. Fülop, Gy. Gróf, Á. Gyenis, R. Kovács, P. Ván, and J. Verhás. Deviation from the Fourier law in room-temperature heat pulse experiments. *Journal of Non-Equilibrium Thermodynamics*, 41(1):41–48, 2016.
- [12] P. Ván, A. Berezovski, T. Fülop, Gy. Gróf, R. Kovács, Á. Lovas, and J. Verhás. Guyer-Krumhansl-type heat conduction at room temperature. *EPL*, 118(5):50005, 2017. arXiv:1704.00341v1.
- [13] A. Fehér, R. Kovács. On the evaluation of non-Fourier effects in heat pulse experiments. *International Journal of Engineering Science*, 169:103577, 2021. arXiv:1704.00341v1.
- [14] A. Fehér, N. Lukács, L. Somlai, T. Fodor, M. Szűcs, T. Fülop, P. Ván, R. Kovács. Size Effects and Beyond-Fourier Heat Conduction in Room-Temperature Experiments. *Journal of Non-Equilibrium Thermodynamics*, 46:403–411, 2021.
- [15] R. A. Guyer and J. A. Krumhansl. Solution of the linearized phonon Boltzmann equation. *Physical Review*, 148(2):766–778, 1966.
- [16] P. Ván. Weakly nonlocal irreversible thermodynamics – the Guyer-Krumhansl and the Cahn-Hilliard equations. *Physic Letters A*, 290(1-2):88–92, 2001.
- [17] P. Ván and T. Fülop. Universality in heat conduction theory – weakly nonlocal thermodynamics. *Annalen der Physik (Berlin)*, 524(8):470–478, 2012.

¹DEPARTMENT OF ENERGY ENGINEERING, FACULTY OF MECHANICAL ENGINEERING, BME, BUDAPEST, HUNGARY ²WIGNER RESEARCH CENTRE FOR PHYSICS, INSTITUTE FOR PARTICLE AND NUCLEAR PHYSICS, BUDAPEST, HUNGARY ³MONTAVID THERMODYNAMIC RESEARCH GROUP